Probabilistic characterizations of flood hazards in deltas

Application to Hoek van Holland (Netherlands)

Diakomopoulos, Faidon; Antonini, Alessandro; Bakker, Alexander Maria Rogier; Stancanelli, Laura Maria; Hrachowitz, Markus; Ragno, Elisa

DOI
10.1016/j.coastaleng.2024.104603

Publication date
2024

Document Version
Final published version

Published in
Coastal Engineering

Citation (APA)
Diakomopoulos, F., Antonini, A., Bakker, A. M. R., Stancanelli, L. M., Hrachowitz, M., & Ragno, E. (2024). Probabilistic characterizations of flood hazards in deltas: Application to Hoek van Holland (Netherlands). *Coastal Engineering*, *194*, Article 104603. https://doi.org/10.1016/j.coastaleng.2024.104603

Coastal Engineering 194 (2024) 104603

Contents lists available at ScienceDirect

Coastal Engineering

journal homepage: www.elsevier.com/locate/coastaleng

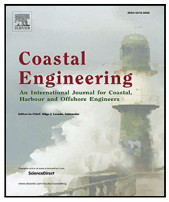

Probabilistic characterizations of flood hazards in deltas: Application to Hoek van Holland (Netherlands)

Faidon Diakomopoulos [a,*], Alessandro Antonini [a], Alexander Maria Rogier Bakker [a,b], Laura Maria Stancanelli [a,c], Markus Hrachowitz [a], Elisa Ragno [a]

[a] Faculty of Civil Engineering and Geosciences, TU Delft, 2628 CN, Delft, The Netherlands
[b] Rijkswaterstaat, Ministry of Infrastructure and the Environment, 3526 LA, Utrecht, The Netherlands
[c] Department of Civil, Architectural, and Environmental Engineering, University of Padova, 35122 Padova, Italy

ARTICLE INFO

Keywords:
Sea level dynamics
Extreme value analysis
Copulas
Tide-surge interactions
Extreme Water Level

ABSTRACT

Coastal flooding events pose a critical risk in delta areas, since they are characterized by population growth and urban expansion. A better understanding of Extreme Water Levels (EWLs), the mechanisms generating them, and their components, i.e., astronomical tide and storm surge is of great importance as they drive the maintenance and design of flood protection systems. Therefore, a statistical investigation of them can provide new insights for more reliable flood risk mitigation infrastructures. In this study, we analyse these components and compare different probabilistic methods i.e., univariate extreme value analysis, copula functions, and Joint Probability Method (JPM) for the better estimation of EWLs. We use Hoek van Holland (NL) as a representative case study, since the dynamic conditions of this deltaic environment with man-made infrastructures render the area of strategic importance. The results indicate that a more accurate estimate of the declustering time between extreme events can be achieved using correlation of high surges and high wind speeds, taking into consideration also the wind direction. In the Southwest Delta this time estimated to be around 4 days. Furthermore, the EWLs components, i.e., surge and astronomical tide, show negative dependence. From the comparison between statistical approaches to model EWLs, results show that EWLs estimated via EVA and JPM do not vary significantly, while copulas' seems to outperform the other methods. However, the selection of the proper copula to show the dependence is critical. As a conclusion, the analysis of the dependence between tides and storm surges can lead to more robust inferences of EWLs.

1. Introduction

Currently, 2.15 billion people live in coastal regions and 898 million in the low-elevation coastal zone (Reimann et al., 2023). Coastal cities and communities have been and will continue to be important economic and trade centres. However, population growth and urban expansion combined with projected Sea Level Rise (SLR) pose a significant threat to such communities (Nicholls, 1995; Woodruff et al., 2013; Neumann et al., 2015; Nicholls et al., 2008). Low-lying delta regions, where different natural processes interact, are under great pressure. For example, Hsiao et al. (2021) showed that the flooded area in Tawain due to coastal flooding can potentially highly increase due to a changing climate. In Europe, the Ebro Delta region (Spain) requires a new flood management strategy to overcome the effect of projected SLR (Grases et al., 2020; Sánchez-Arcilla et al., 2008). In the US, the consequences of SLR in the Mississippi Delta were studied, and the importance of the integrated, long-term management plans was underlined (Day and Templet, 1989). Generalizing the effect in low-lying delta regions on a global scale, Nienhuis and Van de Wal (2021) estimated a loss of ~ 5% of global delta land in 2100 due to SLR.

The Netherlands is situated in the delta of the rivers Rhine, Meuse, Scheldt, and Ems along the North Sea coast. About 26% of the Dutch territory is below mean sea level, and about 60% is vulnerable to floods. Because of the large number of inhabitants and high value of assets, the Netherlands has a high level of protection against flood, provided by a comprehensive system of dams, seawalls, storm surge barriers, dikes, dunes, pumps, sluices, and regular beach nourishments (Van Alphen et al., 2022). In this context, new revisions about the estimation of EWLs (KNMI, 2024) and the effect of SLR that is expected to alter Extreme Water Level (EWL) statistics, pose significant challenges for infrastructure design and risk assessment. These changes raise several issues regarding the suitability of the current management

* Corresponding author.
E-mail address: F.Diakomopoulos@tudelft.nl (F. Diakomopoulos).

https://doi.org/10.1016/j.coastaleng.2024.104603
Received 5 June 2024; Received in revised form 27 August 2024; Accepted 28 August 2024
Available online 31 August 2024

approach (Stijnen et al., 2014) and the operability of current infrastructures (Van Alphen et al., 2022). In the Dutch Southwest Delta, a critical location is represented by Hoek van Holland, where the inlet of the port of Rotterdam, the largest seaport in Europe is located. Here, the Maeslant storm surge barrier protects the Rotterdam harbour and the region of South Holland. The barrier was designed to close on average once every 10 years (Katsman et al., 2011; Van den Brink and de Goederen, 2017). However, the new analysis by the The Royal Netherlands Meteorological Institute KNMI (KNMI, 2024) shows an overestimation of the EWL with the current techniques, calling for a deeper understanding of EWL conditions, their components, and interactions (Antonini et al., 2019).

The observed Water level (WL) is the result of the combination of astronomical tides, driven by astronomical forcing, surge, influenced by weather systems interacting with the topography and morphology of the region, and mean sea level, i.e., the sea level when waves and tidal components are averaged out. Previous studies highlight the importance of dependence between tides and surges for reliable estimations of EWLs (Proudman, 1955a; Rossiter, 1961; Arns et al., 2020; Ragno et al., 2023), but a comparative analysis between dependent, independent and commonly used statistical models for the estimation of extremes is still missing.

Several studies have shown the tendency of the peak of high surges to occur during rising tide (Proudman, 1955a,b; Rossiter, 1961). More recently (Arns et al., 2020) showed that the independence between storm surges and tides, often assumed for design purposes, can lead to an overestimation of EWL of up to 30%. Horsburgh and Wilson (2007) observed a phase difference between the peak of high surges and high tides in UK affecting observed EWLs. In the Adriatic and Tyrrhenian Sea, a negative relationship between high astronomical tide and surge is observed when investigating extreme water conditions (Ragno et al., 2023). On the other hand, Williams et al. (2016) showed the independence between extreme surges and astronomical tides, i.e., meaning that the likelihood of any surge to coincide with any tide is the same when studying stations in UK, North Sea and the east coast of the US. Similarly, EWLs are obtained in UK considering high surges and high tides as potentially coincident (Horsburgh and Wilson, 2007), while another common design approach, more conservative, defines EWL as the sum of Highest Astronomical Tide (HAT) and maximum storm surge (Liu et al., 2010).

In the Netherlands, the probabilistic assessment tools used for EWL assessment on structures, e.g., the Maeslant barrier, are designed for estimating WL as a combination of surges with a trapezoidal shape and tides with a cosine shape (Diermanse et al., 2013; Geerse et al., 2019; Geerse, 2020). For the calculation of EWL the phase difference of 1.5 h between the peaks of storm surges and tides was introduced after a revision for the legal set of instruments for flood risk (Wettelijk Beoordelingsinstrumentarium 2017) (Geerse et al., 2019).

Consequently, since the calculation of EWLs is highly sensitive to the adopted statistical method, we present a comparative study of the methods available in the literature, such as (i)univariate extreme value analysis on observed EWLs, (ii) copula functions (Arns et al., 2020; Ragno et al., 2023; Ferrarin et al., 2022) and (iii) the joint probability method (Pugh and Vassie, 1978). The analysis is carried out by using the 66 years long time series available at Hoek van Holland tide gauge. In preparation for the comparative study, we present a step-wise procedure to investigate observed water levels and derive extreme conditions. More specifically, the extent to which observed water level is affected by Sea Surface Pressure (SSP) and wind speed, which are both considered physical drivers for storm surge generation, is investigated via spectral analysis, coherence function, and measure of dependence.

The remainder of the paper is organized as follows. In Section 2, information about the location, and the importance of the study area, as well as the datasets are presented. The methods used to conduct the analyses are described in Section 3. Afterwards, the results are presented in Section 4. Finally, the main points of discussion and conclusions are presented in Section 5 and Section 6, respectively.

2. Data

We analyse the observed Water Level (WL) in Hoek van Holland (South Holland province, NL). Over the years, multiple man-made interventions, especially targeted to the construction and expansion of the port, have altered the tidal range profile along the coast (Paalvast, 2014), requiring some pre-processing of the data before estimating their statistics (Section 2.1). Sea surface pressure and wind speed and direction, being physical drivers for EWLs, will be analysed as well. A summary of the data used in this paper is presented in Table 1.

2.1. Sea level and its components

The gauge station in Hoek van Holland is located in 51.98°N, 4.12°E (Fig. 1) and at a water depth of around 10 m. Here, the dataset with observations from the Global Extreme Sea Level Analysis (GESLA) version 3 (Haigh et al., 2023) that contains sea water level observations on a global scale (see Sl Figure. 1 in the Supplement) is chosen (Fig. 2).

GESLA contains data with different hourly and sub-hourly frequencies for 1900–2018. However, due to the presence of gaps between 1900–1952, such years are excluded from the analysis. In this study, we select the GESLA dataset, over the Rijkswaterstaat (the executive agency of the Ministry of Infrastructure and Water Management in the Netherlands) dataset, which contains daily measurements, since hourly observations are preferred to describe EWLs.

The frequency of the GESLA dataset varies as follows: 3-h frequency between 1953–1970, 1-h frequency between 1971–1986, 10-min frequency between 1987–2015 and 1-min between 2016–2018. To make the GESLA dataset uniform in terms of temporal resolution, the following procedure is applied: for sub-hourly observations, the average value recorded in one hour is selected; for hourly observations, a linear interpolation between consecutive observations is performed as in Lee et al. (2022) assuming that only minor anomalies in the WL can occur between 1 and 3 h.

2.2. Wind and sea surface pressure

In Hoek van Holland, sea surges are mainly caused by high wind speeds from West and N-NW direction (Diermanse et al., 2013; Groeneweg et al., 2022) that typically coincide with low atmospheric pressure systems (Van Ledden et al., 2014). The latter phenomenon is known to contribute to the WL via the inverse barotropic effect (Weisse et al., 2012) in which the atmospheric pressure and the sea surface height are inversely proportional and the increase of atmospheric pressure leads to WL depression and vice-versa. Therefore, we use contemporaneous wind (Fig. 3) and pressure time series recorded at Hoek van Holland (51.99°N, 4.12°E) during the same time interval of the WL to introduce a process based procedure aimed to identified the appropriated declustering time. The wind and pressure data are made publicly available by the The Royal Netherlands Meteorological Institute (KNMI) for the period between 1981 and 2018. They do not present gaps and have a time resolution of 1 h.

3. Methods

The step-wise approach adopted in this work is summarized in Fig. 4 entailing the following steps: (i) decomposition of observed WL (ii) data homogenization, (iii) spectral analysis aimed to do highlight the underlying components of the different adopted data (iv) coherence and correlation analysis for analysing the causality between meteorological drivers and NTR, (v) extreme value analysis, (vi) copula functions, and (vii) Joint Probability Method (JPM) for deriving statistical properties of EWLs.

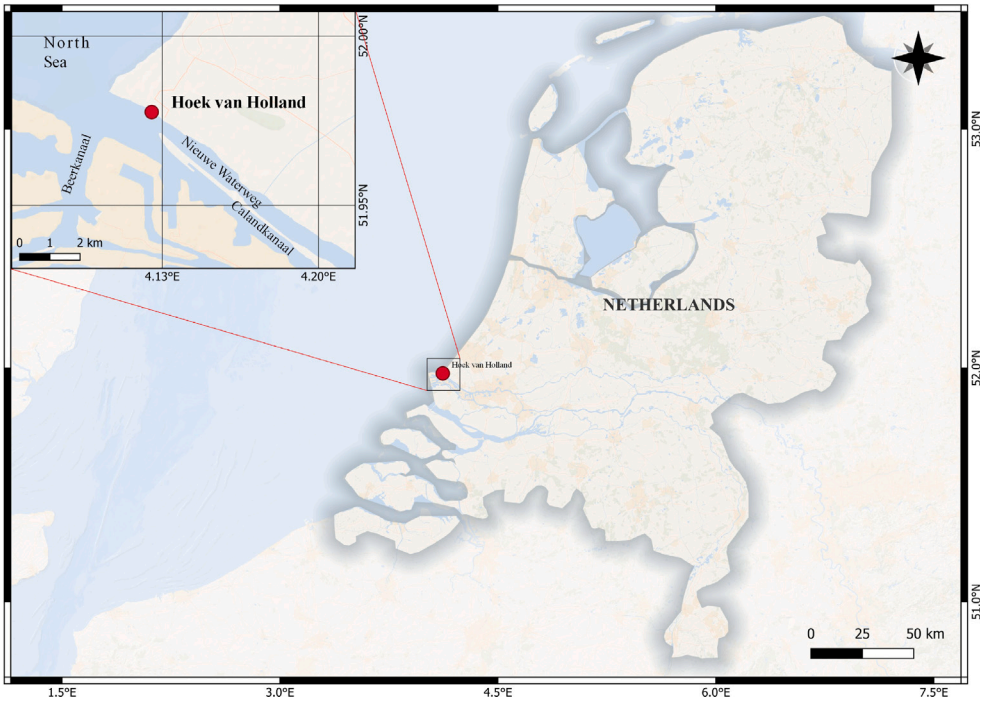

Fig. 1. Hoek van Holland station.

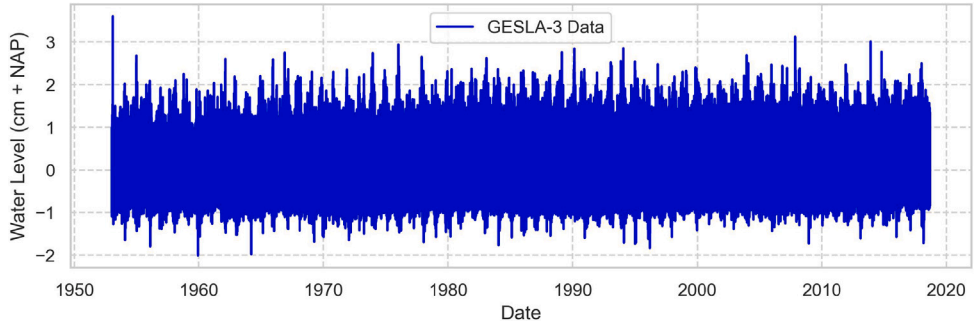

Fig. 2. GESLA-3 data for the Hoek van Holland station. The data are referenced to the Normal Amsterdam Peil (NAP), which is the national reference level for height on land in Netherlands. The maximum observed water level is captured in 01/02/1953 corresponds to the great flood of 1953 and the water reached up to 385 cm+NAP. The second highest peak (318 cm+NAP) that has been recorded in 09/11/2007 was extremely important as it forced to the closing of the Maeslant barrier for first time in a real storm event, since its construction in 1997.

Table 1
Datasets of Water Level, Wind speed and direction, and Surface that have been used within this study.

Dataset name	Period	Time resolution	Deleted years	Total number of years
GESLA-3-Water Level	1900–2018	1-h (reassembled)	1900–1952	66
KNMI-Wind Direction	1981–2018	1-h	–	63
KNMI-Wind Speed	1981–2018	1-h	–	63
KNMI-Surface Pressure	1981–2018	1-h	–	63

3.1. Water level decomposition

Observed WL results from the combination of astronomical tides, surges, regional wave set-up, intra-annual and monthly mean sea level anomalies (interannual variability), an error component and mean sea level (Ferrarin et al., 2022). The mean sea level is assumed equal to the annual mean sea level and includes man-made interventions We use it to homogenize WL (see Section 3.2.) before further decomposing it in astronomical tides and surges. Astronomical tides are considered to be the deterministic component of WL. In this study, they are reconstructed using the toolbox T_Tide by Pawlowicz et al. (2002).

The other components, mainly driven by the meteorological perturbations and the morphology of the area, are then evaluated by subtracting the reconstructed tide from the homogenized WL observations. The results of this operation is hereafter refer as Non-Tidal Residuals (NTR) (Arns et al., 2020; Ferrarin et al., 2022) and it is schematized in Fig. 5.

3.2. Data homogenization and trend's test

Due to the combination of many man-made interventions in Hoek van Holland and possible influence of SLR, homogenization of observed WL (detrending) is necessary to conduct statistical analysis, as

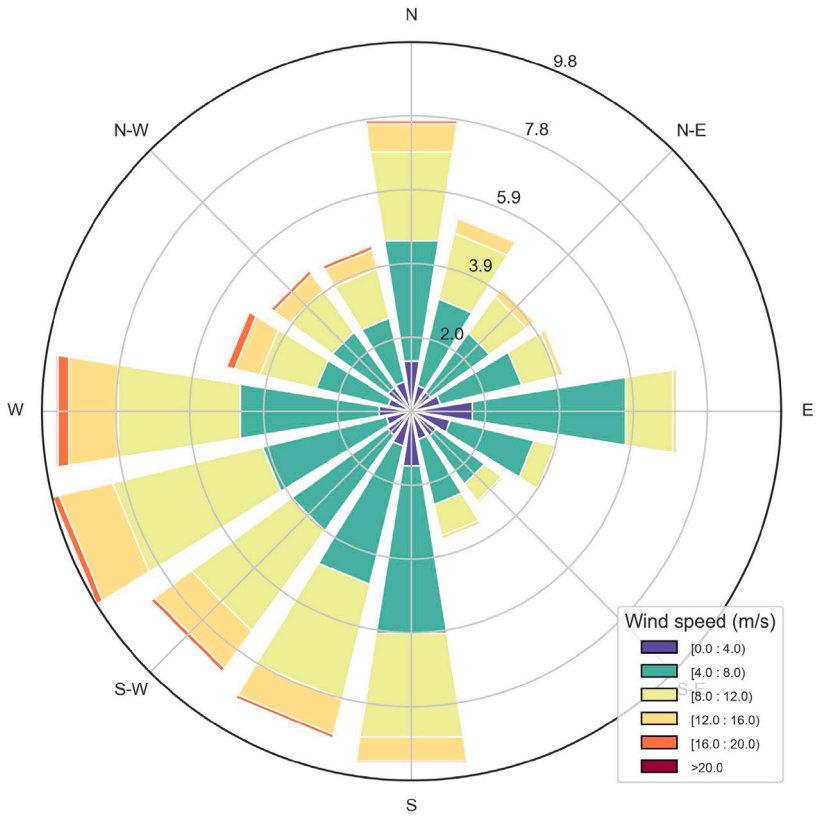

Fig. 3. Wind rose for Hoek van Holland station.

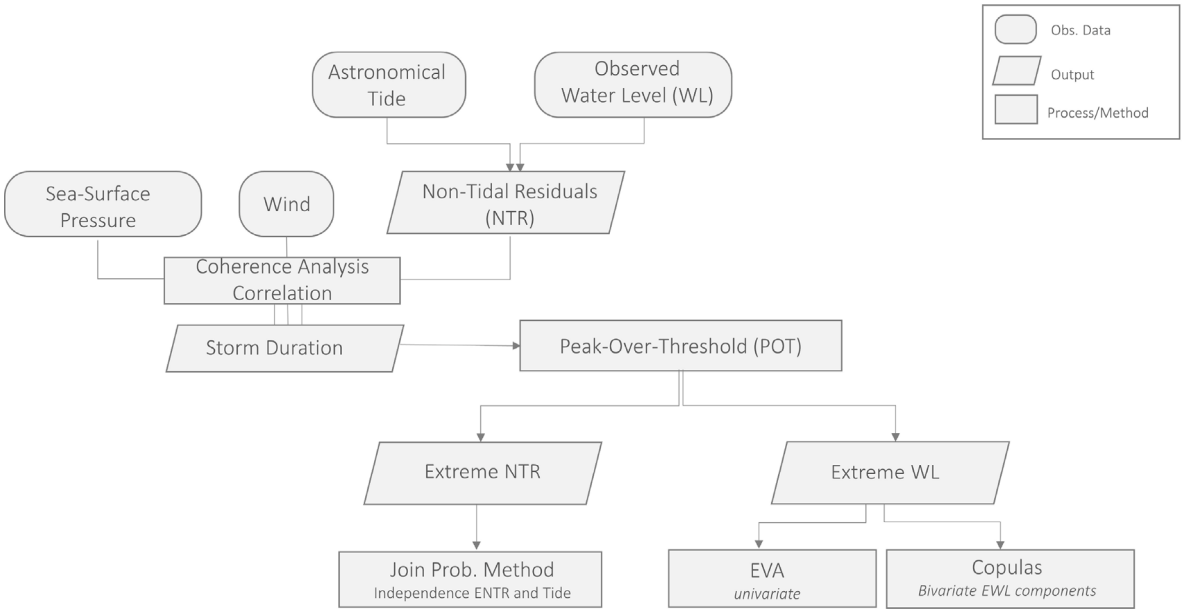

Fig. 4. Flow diagram of the framework of the methodology adopted in this paper. The homogenized Water Level (WL) data have been divided into the tidal and Non-Tidal Residual (NTR) components. For the latter one the wind speed and Sea Surface Pressure (SSP) as the main drivers are analysed to define the duration of storm events. In the probabilistic part of the analysis three different approaches are compared. On the one hand, the Joint Probability Method (JPM) which is oriented by the extreme NTR and the NTR and tides are assumed independent. On the other hand Copulas and Extreme Value Analysis (EVA) are Extreme Water Levels (EWL) oriented, as they have been calculated with Peak Over Threshold (POT), differing in the implementation method as in the first the dependence between tides and NTR is taken into consideration, whilst in the EVA method statistical distributions are fitted directly to the EWL for projection in higher return periods.

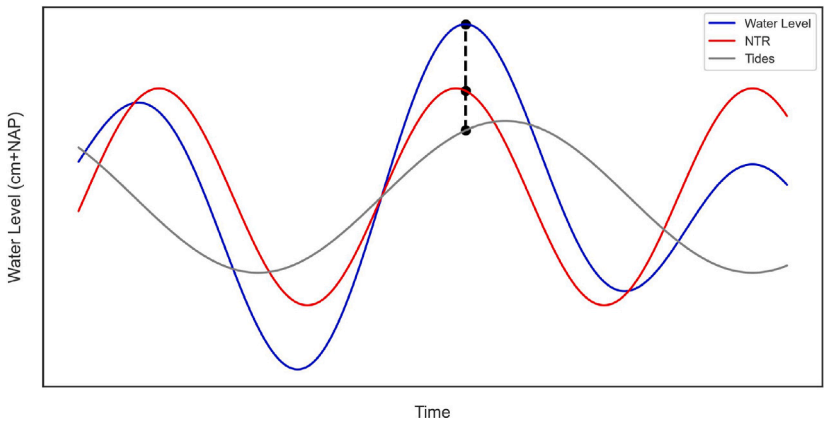

Fig. 5. Explanation of the pair of NTR and tide that is chosen for the analysis. The black dots in NTR and tide timeseries correspond to the peak of EWL at the same time t.

stationary data are needed (Caires, 2011). At the same time, we are interested in evaluating whether MSL presents long-term statistically significant trends. A well known method for trend detection is the Mann–Kendall Test (Mann, 1945; Kendall, 1975) which tests the Null-Hypothesis (H_0) of no-trend in the data against alternatives (Masina et al., 2022). However, the correlation between data can lead to a faulty rejection of H_0 (Yue and Wang, 2004; Sartini and Antonini, 2024). To overcome this issue, the pre-whitening Mann–Kendall Test was introduced by Yue and Wang (2002). In this test, the time series are divided into independent events, and serial correlation is removed. Here, we implement the pre-whitening test at the significance level of $\alpha = 0.05$ to investigate the statistical significance of long-term trends on annual MSL.

The procedure of data homogenization is implemented as follows: (i) Mean Sea Level (MSL) is calculated as the yearly average of hourly WL observations, (ii) different time periods are selected, based on the visual inspection of the trends of MSL, (iii) using the pre-whitening Mann–Kendall Test the presence of trends is tested, (iv) the characteristics of trend-lines (Sen's slope (Sen, 1968) and intercept) for every period and the yearly values from these trend-lines are calculated, (iv) to correct the data to the final year of observations, the difference between the trend-line value of 2018 and every other year is calculated and (v) this difference is added to the initial yearly MSL to make it homogeneous. Finally (vi) the new homogenized yearly MSL is added to every hourly WL observation of this year. With this procedure we ensure stationary and from the correction to the latest year, the possible effect of SLR and man-made interventions is taken into consideration.

3.3. Frequency analysis

To properly describe the energy content within the WL, NTR and tides two different spectral resolution have been tested. The first one is based on Kaiser Bessel window of $N = 8192$ h ($\Delta f = 1/N = 0.00122$ cycles per hour (cph)) with a half-window overlap and degrees of freedom $\nu = 81$. It is used for identifying components with frequencies between $10^{-4} - 1$ cph (see also (Thomson and Emery, 2014; Medvedev et al., 2020)). While with the aim of focusing on the diurnal ($f = 0.033$–0.043) and semidiurnal band ($f = 0.077$–0.085), a Kasser Bessel window of $N = 65,536$ h ($\Delta f = 1/N = 0.000015$ cph) and a half-window overlap, is applied, allowing us to observe details about these components (Medvedev et al., 2017).

Sea surface pressure conditions are a critical factor in the generation of storm surges (Ferrarin et al., 2022; Woodworth et al., 2019). For this case, a spectral Kaiser Bessel window of $N = 65,536$ h has been selected to show more details in the frequency domain of the possible declustering time (0.01–0.03 cph, or 1.4–4.2 days).

3.4. Statistical models for EWLs

We are interested in investigating EWLs and their statistics since they drive infrastructure design and risk assessment procedures. In the following we first describe how we implemented the Peak Over Threshold method to identify extreme events. Then we describe the three different statistical models, i.e., extreme value analysis, copulas functions, and joint probability method, used to derive high return period quantiles and potential design values associated with low probability of occurrence.

3.4.1. Peak over threshold

Peak Over Threshold (POT) method is a widely used approach for sampling extremes when dealing with sub-daily samples or when few years of observations are available (Ragno et al., 2018, 2019; Antonini et al., 2019; Raby et al., 2019).

Following the POT approach, a threshold u should be defined and excesses above such threshold are considered extremes. Threshold selection can be a quite challenging task and many different methods have been proposed. Graphical methods such as Mean Residual Life Plot (Davison and Smith, 1990) and Parameter Stability Plot (Teixeira et al., 2018; Caires, 2011) can be used to select the appropriate threshold via visual inspection and as a result difficulties might be encountered when assessing the influence of small changes. Besides the graphical methods, approaches that automate the threshold selection have also been proposed e.g., Solari et al. (2017) while others propose techniques designed to reduce the sensitivity to the choice of a single threshold e.g., Northrop et al. (2017). Other authors (Ferrarin et al., 2022; Arns et al., 2020; Wahl et al., 2017) proposed the use of the percentiles values, e.g. from 99th to 99.9th, to identified most suitable threshold value. It is worth noticing that the latter depends on the record length and even if it is widely used it is difficult to be justified scientifically. Here, a threshold of 212.2 cm is chosen, following the Dutch standards for EWL generated by the most severe storms which are from NNW direction (Diermanse et al., 2013). In the GESLA dataset used for the analysis, this value corresponds to the $\approx 99.9th$ percentile. Hence this threshold is chosen as it combines the theoretical percentile method with the practical flood protection standards. When the JPM is implemented, NTR peaks are selected via POT with a threshold of 107.6 cm, based on the stability parameters plot and mean residual life plot (see Sl Figure. 12 in the Supplement), since no other information is available. This threshold value corresponds to the $\approx 99.5th$ percentile of NTRs.

3.4.2. Storm duration-declustering time

To infer the statistics of the extremes, such extremes should be independent, i.e., should come from independent events. To ensure the independence between selected peaks, a declustering time between

two consecutive peaks should be selected. Usually, the declustering time is assumed related to the length of the storm. In this work it is assumed equal to the average storm duration at the location of the tide gauge. Previous literature about declustering time in Hoek van Holland has reported 2.41 days as the time between two independent storm events (Dillingh et al., 1993), while more recent reports have seen that peaks with a time difference less than 4 days can be considered belonging to the same event (Caires, 2011). A recent global study by Martín et al. (2024) suggests the storm duration at nearby gauges to Hoek van Holland close to 4 days.

In the effort to identify a declustering time we attempt to estimate an average duration of the extreme storm surge events. First the coherence function is used to investigate the frequencies for which two variables show the highest degree of dependence. Here, we use it to estimate the declustering time in the Peak-Over-Threshold (POT) analysis. This is because we expect to identify non-negligible correlation between NTR and sea surface pressure due to the causality relation between these variables. More specifically, the storm duration (and so the declustering time) is assumed to be equal to the frequency of the highest coherence. The coherence function is given by the following equation:

$$C_{xy}(f) = \frac{|G_{xy}(f)|^2}{G_{xx}(f)G_{yy}(f)} \tag{1}$$

where, $G_{xx}(f)$ and $G_{yy}(f)$ are the power spectra of NTR and surface pressure, respectively, and $G_{xy}(f)$ is the cross-power spectrum between them. The range of $C_{xy}(f)$ varies from 1 which corresponds to perfectly related variables to 0 which means that there are no causality between them.

Extreme storm surges (extreme values of NTRs) are driven by high wind speed. Hence, we quantify the dependence between NTR and wind speed by means of correlations, i.e., Spearman's ρ_s to identify the declustering time. The following steps are needed: (1) Implementation of the POT approach for NTRs with a threshold of 107.6 cm (same as the threshold for JPM) and three different declustering times of 3, 4 and 5 days. (2) Selection of time windows from 12 (±6) to 72 (±36) hours based on the time of the peak NTRs from POT method, (3) finding the maximum wind speed inside these time windows and (4) calculation of the non-parametric Spearman's rank correlation coefficient ρ_s for peaks of NTR and wind speed (see Fig. 6). The declustering time on which the correlation reaches its maximum value is the estimated one for the Peak Over Threshold. Previous contributions showed that along the Dutch coast, extreme storms are generated by westerly and northwesterly winds (Horsburgh and Wilson, 2007; Diermanse et al., 2013; Van den Brink and de Goederen, 2017). To investigate the contribution of wind direction in the correlation we chose several direction windows, finding the wind speed peaks as previously, dependently on the corresponding wind direction windows. From the results the direction window between 270° and 360° that led to highest values of correlation is 310° to 330°.

In this study, we use the results of the coherence analysis between NTR and surface pressure and the correlation between NTR and wind speed to select a representative declustering time equal to 4 days.

3.4.3. Extreme value analysis

Extreme Value Analysis (EVA) is a method to determine the statistical characteristics of observed extreme events and infer low-probability events, often not observed, such as those occurring on average once every 1000 or 10,000 years.

The distributions tested to model excesses of WL and NTR, i.e., Generalized Pareto, Weibull for minima, Exponential, and Generalized Gamma, are listed in Table 2.

The threshold excesses, e.g. excesses selected based on the POT method, belong to the generalized Pareto family (Coles et al., 2001). The value of shape parameter ξ in Generalized Pareto Distribution (GPD) (Table 2) determines its qualitative behaviour: for $\xi = 0$ it has a Type I tail, corresponding to the exponential distribution; for $\xi > 0$ it has a Type II tail and it is the Pareto distribution; and for $\xi < 0$ it has a Type III tail it is a special case of the beta distribution. However, a previous study of Caires (2011) on EWL in Hoek van Holland, showed that the shape parameter of GPD is quite small, albeit non-0. This could be an indicator of a type II — exponential distribution. As the exponential distribution is a special case of the Weibull for minima distribution with a shape parameter ($c = 1$), the latter one is also investigated (Table 2). As a matter of fact, it is expected that the Weibull distribution fits better the data given the extra parameter. Similarly, the Generalized Gamma distribution being a generalization of the Weibull distribution with one more shape parameter α, is also tested.

Table 2
Tested Distributions. $f(y)$ indicates the probability density function (pdf); y the excesses above the threshold obtained as the difference between the observations (x) and the selected threshold.

Name	Mathematical description	Parameters
Generalized Pareto	$f(y) = (1+\xi\frac{y}{\sigma})^{-1-\frac{1}{\xi}}$	$y \geq 0$ σ scale $\xi \in \mathbb{R}$
Weibull	$f(y) = c(\frac{y}{\sigma})^{c-1}\exp(-\frac{y}{\sigma})^c$	$y \geq 0$ σ scale c shape $c > 0$
Exponential	$f(y) = \exp(-\frac{y}{\sigma})$	$y \geq 0$ σ scale
Generalized Gamma	$f(y) = \frac{k(\frac{y}{\sigma})^{ka-1}exp(-(\frac{y}{\sigma})^k)}{\Gamma(a)}$	$y \geq 0$ σ scale k,a shape $k, a > 0$

The Maximum Likelihood Estimation (MLE) method is implemented to estimate the parameters of the distributions. In this study, three goodness-of-fit (GoF) metrics are performed to assess which distribution best represents the observations: Root Mean Square Error (RMSE); Kolmogorov–Smirnov test (K–S); and the Akaike Information Criterion (AIC).

The first GoF metric is Root Mean Square Error (RMSE):

$$RMSE = \sqrt{\frac{1}{N}\sum_{n=1}^{N}(y_i - x_i)^2} \tag{2}$$

where N is the total number of values, y_i and x_i are the predicted and observed values, respectively. A smaller number of this error indicates a better fit.

The other GoF metric is the Kolmogorov–Smirnov test (K-S) Eq. (3)

$$D = max|F_{obs}(x) - F_{est}(x)| \tag{3}$$

where the statistic D describes the maximum distance between $F_{obs}(x)$ and $F_{est}(x)$ which are the empirical cumulative distribution function (cdf) of the observations and the theoretical cdf, respectively. The smaller the test statistic the better the fit.

These two metrics have been previously use in several works addressing wind extreme values analysis (Dookie et al., 2018; Kollu et al., 2012) and waves (Naderi and Siadatmousavi, 2023).

The extra parameters in distributions increase their flexibility but also entail more uncertainty in the parameter estimation, making them more complex. Consequently, it is important to estimate not only how good a distribution with more parameters fits to the data but also the number of parameters that are needed for this. For that reason, the Akaike Information Criterion (AIC) is used.

$$AIC = 2(k - lnL) \tag{4}$$

where L is the likelihood function and k is the number of parameters of the model. The former can be seen as a penalization score for more complex distributions, i.e., with a higher number of parameters. The best distribution is the one with the smallest AIC.

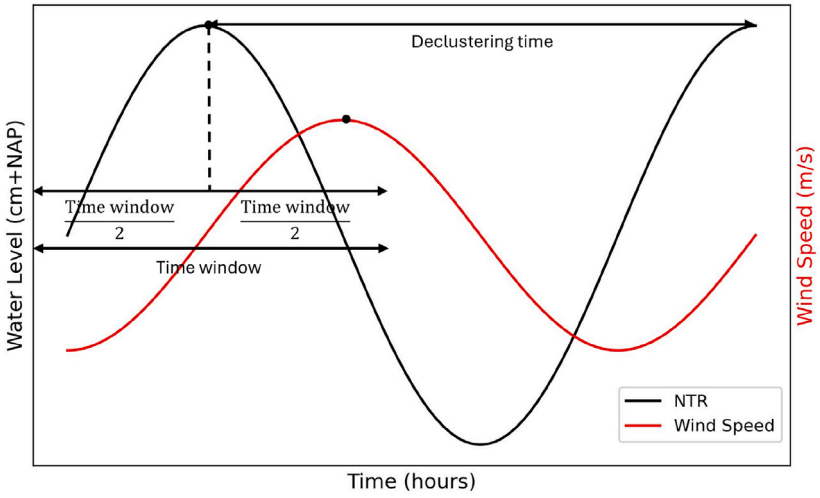

Fig. 6. Explanation of the declustering time selection method based on correlation NTR and wind speed. The declustering time determines the time difference between independent NTR peaks. The time window/2 represents the time before and after the NTR peak during which the highest wind speed peak is correlated with the corresponding NTR peak (depicted by black dots).

3.4.4. Copulas

Copulas are flexible statistical tools for modelling the joint probability of dependent variables. More specifically, if the two variables X, Y, with marginal distributions F_X and F_Y, respectively, show a level of dependence, their dependence structure can be modelled via copula function C independently of their marginal distributions. Their joint distribution can be written as:

$$F_{X,Y} = C(F_X(x)F_Y(y)) \tag{5}$$

where C is a copula uniquely defined for continuous F_X and F_Y (Sklar, 1973).

In this study, we first assess if EWL components, NTR and tide, are statistically dependent based on non-parametric Kendall's rank correlation coefficient τ, (Kendall, 1938):

$$\tau = \frac{N_{cp} - N_{dp}}{N_p} \tag{6}$$

where N_{cp} is the number of concordant and N_{dp} the number of discordant pairs, respectively, and the sum of them $N_{cp} + N_{dp} = N_p$ the total number of pairs N_p. The pair of observations X, Y (in our case NTR and Tide) refers to (x_i, y_i) and (x_j, y_j) where $i < j$ and is defined as concordant if the sort order of (x_i, x_j) agrees with (y_i, y_j), otherwise it is called discordant. Its values vary between -1 for completely negative correlation, to $+1$ for positive, respectively. A value of 0 expresses no ordinal correlation between observations.

If the dependence is statistically significant (0.05 significance level), then the best theoretical copula is selected based on the AIC, from the following families: Gaussian, Student, Clayton, Gumbel, Frank, Joe, BB1, BB6, BB7 and BB8.

Moreover, to investigate the effect of explicitly modelling the dependence between the variables, the independence copula is derived to assess the effect of modelling the dependence between NTR and tides on EWLs. To do so, we compare EWLs randomly generated from the best theoretical copula and EWLs randomly generated from the independence copula. More specifically, 10,000 pairs of dependent X_{dep}, Y_{dep} are sampled from the selected best copula, and 10,000 pairs of independent X_{ind}, Y_{ind} are sampled from the independence copula. EWLs in all the cases are obtained by the sum of the two components.

3.4.5. Joint probability method

The Joint Probability Method (JPM) was first introduced by Pugh and Vassie (1978) and estimates the distribution of EWL via the convolution of the Cumulative Distribution Function (CDF) of the NTR and the Empirical Probability Density Function (EPDF) of the high tides.

$$F(z) = \int G(z - x)f(x)dx \tag{7}$$

in which F is the distribution of estimated EWL, G is the distribution of extreme NTRs, obtained via POT, and f the empirical distribution of high tides. The underlying assumption of this method is that NTR and tides are independent.

4. Results

4.1. Water level dynamics

We first show the results of the MK trend test on the observed water level in Hoek van Holland. Then, we quantify the storm duration (and so the declustering time for the POT analysis) based on the correlation between wind and NTR and coherence analysis between sea-surface pressure and NTR

4.1.1. Trend analysis using pre-whitening Mann Kendall test

The annual mean water levels (Fig. 7) show jumps and monotonic trends due to man-made interventions and sea level rise.

We observe two main jumps: (1) in 1965 associated with the works for Maasvlakte 1 and industrial area (Paalvast, 2014; Caires, 2011); and (2) in 1990 caused by the connection between the Harteelkanaal and Beerkanaal. Before 1965, the pre-whitening MK shows no trend ($pvalue = 0.27$). Between 1965 and 1990 the trend is statistically significant with a $slope = 0.35$ cm/year ($pvalue = 0.033$). between 1990 and 2018 the trend is still statistically significant ($pvalue = 0.027$) but with a milder $slope = 0.1$ cm/year.

4.1.2. Spectral analysis and coherence

From the spectra of Water Level (WL), NTR, and tide (Fig. 8a), the NTR spectrum shows the lowest energy in the diurnal and semidiurnal bands (shaded red area), as NTR is calculated by removing astronomical tides from WL. However, NTR still shows some energy around the tidal components which can be attributed to NTR-tide interaction. At the same time, WL in these bands is governed by astronomical tides, so WL and tidal energies almost coincide. By zooming in into the diurnal band, Fig. 8b, the WL most predominant constituent is O_1. The other components influencing WL are the K_1 and P_1 components, connected to the sun's declination, and the Q_1 component, related to the elliptical orbit of the moon. By zooming in into the semi-diurnal band, Fig. 8c, the WL most predominant constituent is M_2, which is also the most

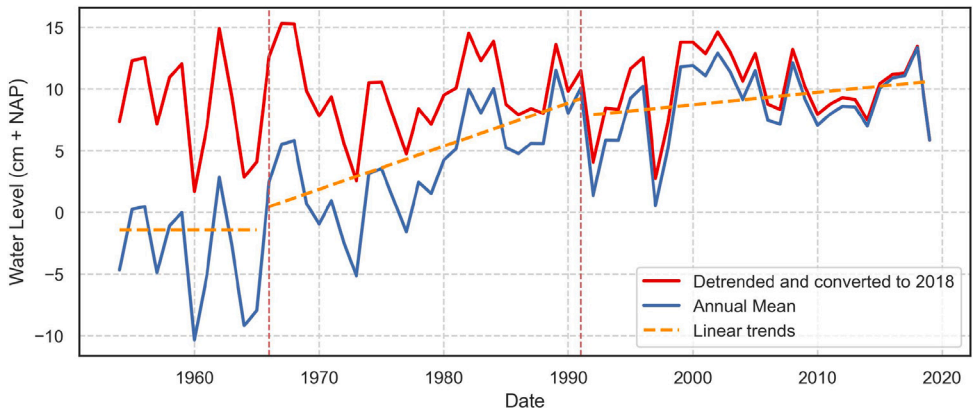

Fig. 7. Annual mean sea level. The dashed orange lines indicate the linear trend. The red line is the annual mean homogenized to the last year of observations (2018).

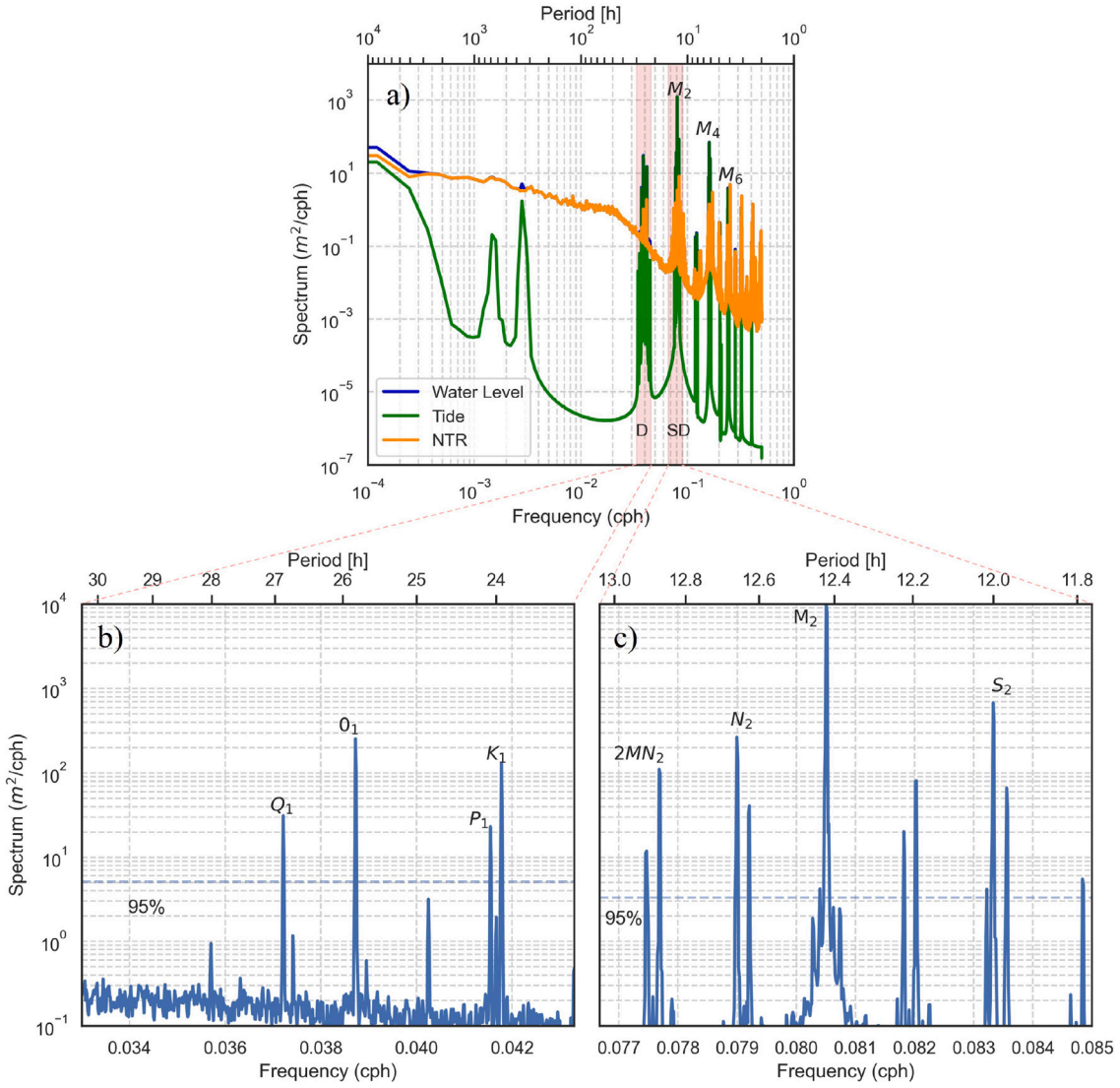

Fig. 8. Panel (a) shows the spectral analysis for the total water level (blue solid line), NTR (orange solid line), and tides (green solid line). The light red shaded areas represent the diurnal and semi-diurnal bands. Panels (b) and (c) show the WL spectra within the diurnal and semi-diurnal bands, respectively. In panels (b) and (c) the dashed line corresponds with the 95% confidence level and the most influenced harmonic constituents are highlighted (O_1, K_1, Q_1, P_1 and M_2, S_2, N_2, $2MN_2$, respectively).

predominant in the entire spectrum. Around M_2, other sharp peaks are observed which could be linked to the "tidal cusps" generated by the non-linear interaction between tides and mean sea level (Munk et al., 1965). Another important component is the $2MN_2$ resulting from the interaction between M_2 and N_2 due to frictional non-linearity (Teng et al., 2023). At lower frequencies, the WL harmonic constituent M_4 (Fig. 8a), proportional to $(M_2)^2$ (Gräwe et al., 2014), is the second highest peak in the spectrum, (f = 0.17 cph). This can result from the

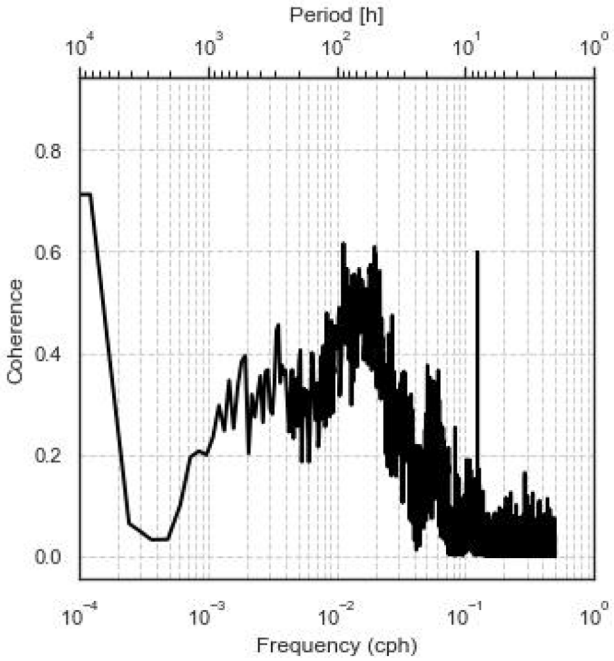

Fig. 9. Coherence between Non Tidal Residuals (NTR) and surface pressure.

interaction with M_2 occurring in estuary regions worldwide (Prestes et al., 2017; Guo et al., 2019). The third highest peak in the spectrum is the constituent M_6 ($f = 0.25$ cph), which is a shallow water harmonic. This peak can be explained by the influence of the river discharge which significantly redistributes the energy from principal tides to overtides (Guo et al., 2015). The remaining peaks may be generated by the influence of seiches in the area (Pattiaratchi, 2011) or by the interaction between surges, tides, and river water (Spicer et al., 2019).

We also analyse the spectrum of SSP (see Sl Figure. 2 in the Supplement). Here, we observe a predominance of semi-diurnal surface pressure variation, similar to the tide spectrum. From the graph, it is difficult to observe peaks in lower frequencies than in diurnal areas.

4.2. Water level extremes

4.2.1. Declustering time and storm duration

To derive EWLs, we first need to determine the declustering time, which we assume is equal to the storm duration. We do so by analysing the coherence between NTR and SSP and the correlation between NTR and wind speed.

Regarding the results of coherence between NTR and SSP, the most interesting finding from Fig. 9 is the frequency band (0.01–0.02 cph) or in a period scale, from 50 to 96 h, in which the coherence is slightly higher than 0.6 identifying the highest causality between NTR and surface pressure. The period of 96 h shows the highest peak in the coherence plot. We use this as an indicator of the typical storm duration.

Both storm duration and wind direction are critical elements to identify and model EWLs. Hence we explore via measure of correlation the dependence between extreme NTR, the meteorological component of WL, and wind speed during storm events.

The north-west direction window considered here (310°–330°) is chosen because it leads to the highest correlation between wind speed from that direction and NTR.

Figs. 10 and 11 show Spearman's correlation coefficients between extreme NTR and wind speed for different declustering times and lag-times between NTR and wind peaks. Correlation coefficients are positive and statistically significant ($pvalue = 0.02$). The highest correlation between NTR and wind is $\rho = 0.49$ assuming 4 days of declustering time and 24 h (±12) of lag between NTR peak and wind peak, regardless of the wind direction (Fig. 10). Such correlation increases to $\rho = 0.61$ for 18 h time window when the wind direction window is considered, assuming 4 days of declustering time. In general, we see that the declustering time of 4 and 5 days provide similar results in terms of correlation coefficient.

Following the results of the coherence between NTR and SSP and the correlation between NTR and wind speed, we assume 96 h (or 4 days) as declustering time in POT analysis to guarantee the independence between extreme events.

Table 3
Values of RMSE, K-S and AIC for the EVA distributions.

Distribution name	RMSE	K-S	AIC
Generalized Pareto	0.399	0.056	1045.9
Weibull	0.396	0.064	1045.4
Exponential	0.399	0.056	1043.9
Generalized Gamma	0.394	0.056	1046.4

4.2.2. POT analysis of WL and NTR

We apply the POT method to WL and NTR to derive statistical properties of EWLs based on the three selected methods, i.e., extreme value analysis, copula functions, and Joint Probability Method (JPM).

In the case of WL, we apply a threshold of 212.2 cm and a declustering time of 4 days. We obtain 124 EWL independent events over 66 years of the given observations, meaning that we have 1.88 event/year. EWL mean is 236.6 cm and the contribution of the corresponding mean NTR is ≈ 137 cm or 58% and from the tidal one 99.6 cm or 42%, respectively (Fig. 12). Moreover, when EWL is decomposed into its components, NTR and tide, are negatively dependent (Fig. 13), meaning that, generally, high values of NTR correspond to low values of tide, and vice-versa. The Kendall's tau correlation coefficient is equal to $\tau = -0.50$ and is statistically significant ($pvalue = 0.02$). From a physical perspective, the observed negative dependence could be explained by the shallow water conditions on an estuary and the effect of the bed friction which leads to higher surge height in rising water and lower in high waters (Proudman, 1955a,b; Rossiter, 1961). Similar results in terms of negative dependence between NTR and tide have been observed in the Adriatic sea with shallow water conditions (Ragno et al., 2023; Ferrarin et al., 2022) and worldwide (Arns et al., 2020).

In the case of NTR, we consider a threshold equal to 107.6 cm and a declustering time of 4 days. This leads to 346 events.

4.2.3. EVA

We first derive EWL statistics using univariate EVA distributions. We fit the distributions in Table 2 to EWLs (Sl Figure. 9 and 10). The GoF tests show that the distributions fit the data well, Table 3. The GP distribution ($\xi = 0.014$ and $\sigma = 24.013$) and the exponential distribution ($\sigma = 24.366$) generally perform best across the three GoF tests (RMSE, K-S, and AIC). The 10,000-year event is 466.2 cm for GP and 452 cm for the exponential one (Fig. 14). Moreover, we observe that the exponential distribution has a smaller confidence interval in contrast with the GP distribution, probably due to the absence of the shape parameter, Fig. 14c. Due to the minor differences in GOF metrics, as all the distributions represent the data well, we use the GPD (Fig. 14a) to compare the results, aligning with the literature (Coles et al., 2001; Caires, 2011).

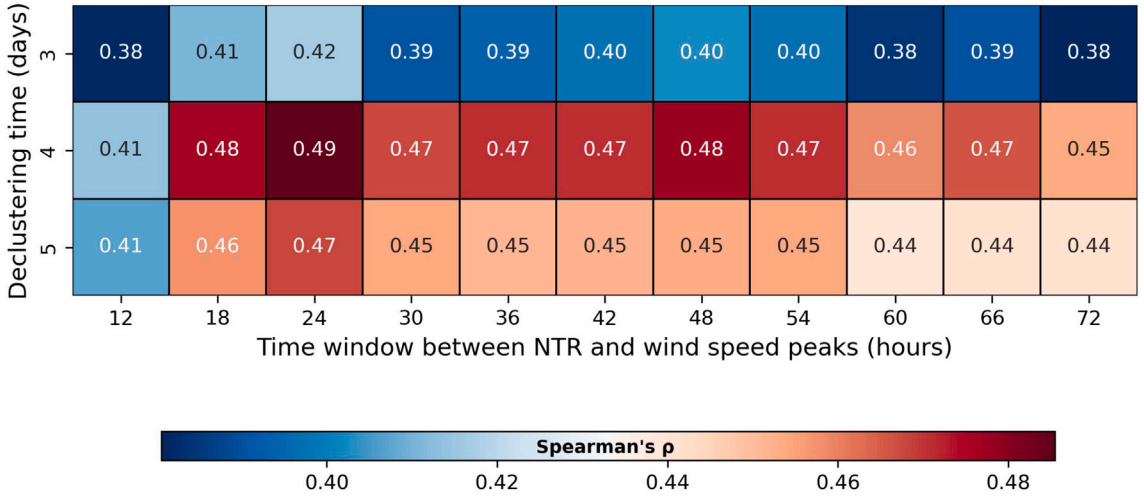

Fig. 10. Spearman's correlation coefficient heatmap for Non Tidal Residuals above 107.6 cm and wind speed irrespective of the wind direction.

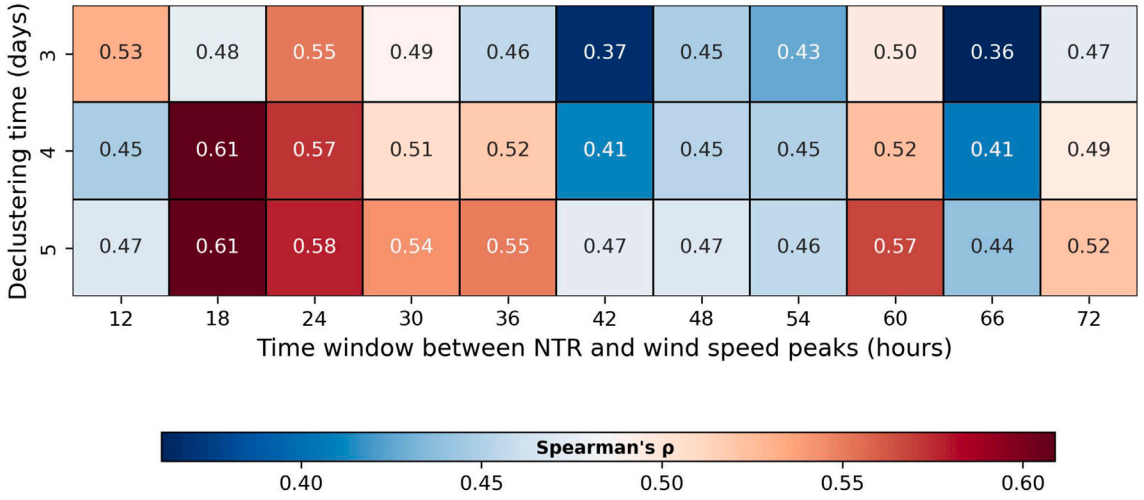

Fig. 11. Spearman's correlation coefficient heatmap for Non Tidal Residuals above 107.6 and wind speed for winds blowing between 310° and 330°.

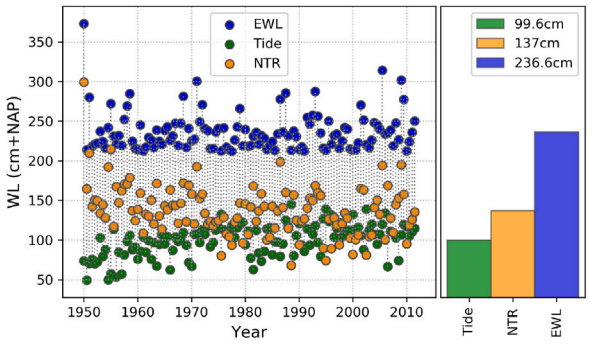

Fig. 12. In the left graph the Extreme Water Levels (EWL) which exceed the threshold of 212.2 cm are shown, as well as their NTR and tide components. On the right graph, the bars represent the mean of these values. The EWL is decomposed into the tides and NTR, so the mean of EWL is the sum of the means of the other two components, as given in the bars.

4.2.4. JPM

We then obtain EWL statistics from the convolution of NTR peaks and high astronomical tides distributions following the JPM method (Pugh and Vassie, 1978). We fit the NTR excesses to the GP distribution. We obtain a distribution with a shape parameter $\xi = -0.062$ and a scale $\sigma = 31.456$. High tides are modelled via empirical pdf (Sl Figure. 14). Fig. 14a shows a good agreement between observations (black dots) and the theoretical distribution from JPM (blue solid line), even though the JPM tends to be unbounded for high values of return periods due to negative shape parameter ξ.

4.2.5. Copulas

The last adopted method to obtain EWL statistics is via copula functions, by modelling the dependence between the components of EWLs, i.e., NTR and tides.

We select empirical marginals for NTR and tides, since we could not identify a suitable theoretical distribution (see Sl Figures. 15 and 16). Once the margins are transformed to be uniformly distributed via the empirical cdf, we fit all the possible copula families available. The theoretical copula with the smallest AIC is the rotated (270 degrees) BB1 copula, followed by the Student and the Gaussian copulas, Fig. 14b. The BB1 copula is one of the Archimedean copulas, and as a result a rotation is needed to allow negative dependence (De Luca and Rivieccio, 2023). The difference between BB1 and elliptical copulas, i.e. Student and Gaussian, is that the former is characterized by reflection asymmetry (Krupskii and Joe, 2013), whilst the other two are symmetric. In the higher quantiles Fig. 14b, this difference is attributed to the presence of some density in the upper right corner (high values

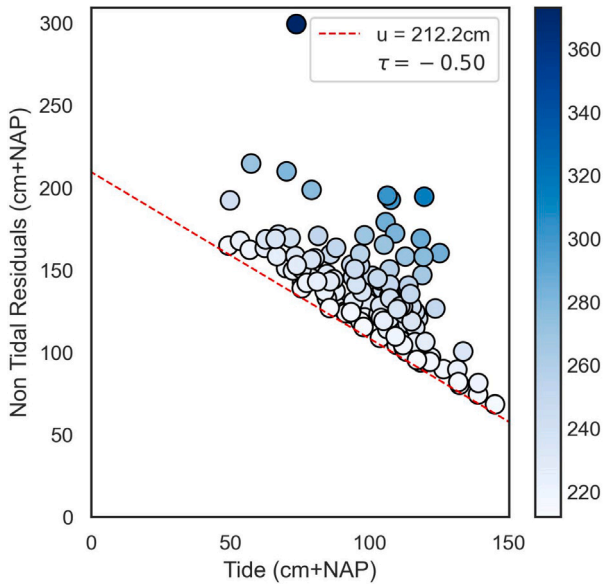

Fig. 13. Scatter plot of the EWL components, i.e., NTR and tide. The colorbar indicates EWL values: darkest colours correspond to higher EWLs, while the lighter colours to smaller EWLs.

of tides and NTR) of the BB1 copula compared to the Gaussian copula where all the density is along and around the $y = -x+1$ line (Sl Figure. 17). We also modelled the case of the independence copulas, Fig. 14b solid light-blue line. We observe a general overestimation of EWL when the observed dependence between NTR and tide is neglected. This is because there are no constraints in the association between high values of tides and NTR in the dependence model.

4.2.6. Comparison between methods

By comparing the three methods, we observe a general agreement between them, Fig. 14a. All the methods seem to reasonably describe the observations (black dots). JPM (blue solid line) seems to overestimate EWL, while the empirical copula seems to underestimate EWL especially for high quantiles.

When we extrapolate to higher quantiles, EWLs modelled via empirical and Gaussian copulas are generally lower than the other methods, Fig. 14b. For the empirical copula, the 10.000 years event is 365.7 cm, which is smaller than the highest observed EWL of 373.04 cm, as the empirical copula is not appropriate for extrapolation. On the contrary, when extrapolating from the rotated BB1 copula, given its specific formulation, the 10.000 years event is 400.9 cm. Special attention should be given to estimating the return period of the extreme water level corresponding to the 1953 extreme event. Recently, the KNMI revised this phenomenon's return period from 500 to 1000 years (KNMI, 2024). Evaluating the different methods for the estimation of the return period of this event, the GP distribution in EVA method leads to an estimation of RP 356 years, and from JPM RP = 301.4 years. Based on KNMI findings these two methods overestimate this event, whilst its corresponding return period from BB1 copula is RP = 1006.11 years, well in agreement with the revised KNMI result. Confirming the needs to account for the dependence between NTR and tide, reliable estimations of EWLs can be extracted via copulas, avoiding the overestimation of the other methods.

Moreover, we observe differences in the amplitude of the confidence intervals due to the different data types needed in each model. In the EVA method, 124 events are used to derive the statistical properties of EWL while in the JPM method, 346 events are adopted. This leads to a confidence interval for the JPM (blue shade) smaller than the EVA (red shade). In the copula method, EWL is modelled via the joint occurrence of its components. This leads to a natural bound for EWL, i.e., the sum of the maximum values of its components, 444.4 cm, and a generally narrower confidence interval than the JPM and EVA methods.

5. Discussion

To carry out this comparative analysis of statistical methods for EWLs, multiple assumptions have been made when processing the data which can affect the results.

Declustering time and threshold selection for POT. Preliminary analyses showed that EWLs are more sensitive to the threshold selection than to the declustering time (Sl Figure. 7 and 8). In this work the selection of the threshold value is based on the previous works. From the analyses on the declustering time, which is here assumed to be average storm duration, we observed that the correlation between wind and NTR vary for declustering periods between 3 to 5 days but it gets stronger when wind direction is considered, i.e., 310°–330°. This could suggest an analysis based only on EWLs generated from northwesterly winds. However, we do not expect great variability in the statistical results, since the majority of the EWL events here selected are generated by northwesterly winds.

EWL and 1953 event. The maximum EWL recorded is the flood event of the 1953 in the North Sea. Its value greatly deviates from the remaining observations (Fig. 14a - grey dots). However, this event is of great importance for infrastructure design in the Netherlands. Indeed, the Deltaworks were designed to prevent disasters such as the ones occurred during that event. All the three methods underestimate such events, i.e., in Fig. 14a - grey dots) all the solid lines are below it. Neglecting the 1953 would have improved the quality of the fitting of the three methods. However, we decided to keep it in the used sample given its great practical importance. In the current study, more flexible methods such as the GP distribution and the theoretical rotated BB1 copula capture better such event as it is included in their confidence intervals.

Comparative Analysis. Small differences are observed when comparing the three approaches and such differences are mainly related to the underlying assumptions of the specific method. Univariate EVA remain still the simplest method, requiring only the WL dataset to be implemented. The JPM method models NTR rather than EWL, under the assumption that NTRs are equally likely to occur with any tide. This leads to a slight overestimation of EWLs. However, such methods require a greater computational effort, and the convolution is sensitive to the selection of the pdf of astronomical tide. The copula model showed some limitation when estimating EWLs since the statistical properties of EWL are derived from modelling the statistical properties of its components, i.e., tide and NTR, and their dependence structure. This introduces more challenges and uncertainties because of the inclusion of additional modelling assumptions. On the other hand, the data are better described by splitting the water level observations into two components, describing their statistical behaviour and their combination. As a result, this approach allows for the construction of a more flexible framework to characterize the overall extremes. At the same time, this approach provides greater insight into tide and NTR components for extreme sea states which cannot be retrieved by the other methods. From the comparison of the results of the methods new insights about the description of EWLs can be provided by the copula approach, potentially increases the accuracy of extrapolated EWLs. It is also worth noticing that the dependence modelled by the copula by fitting it to the components of observed WLs surely encapsulates the physical interaction between tide and surge in the estuarine environment.

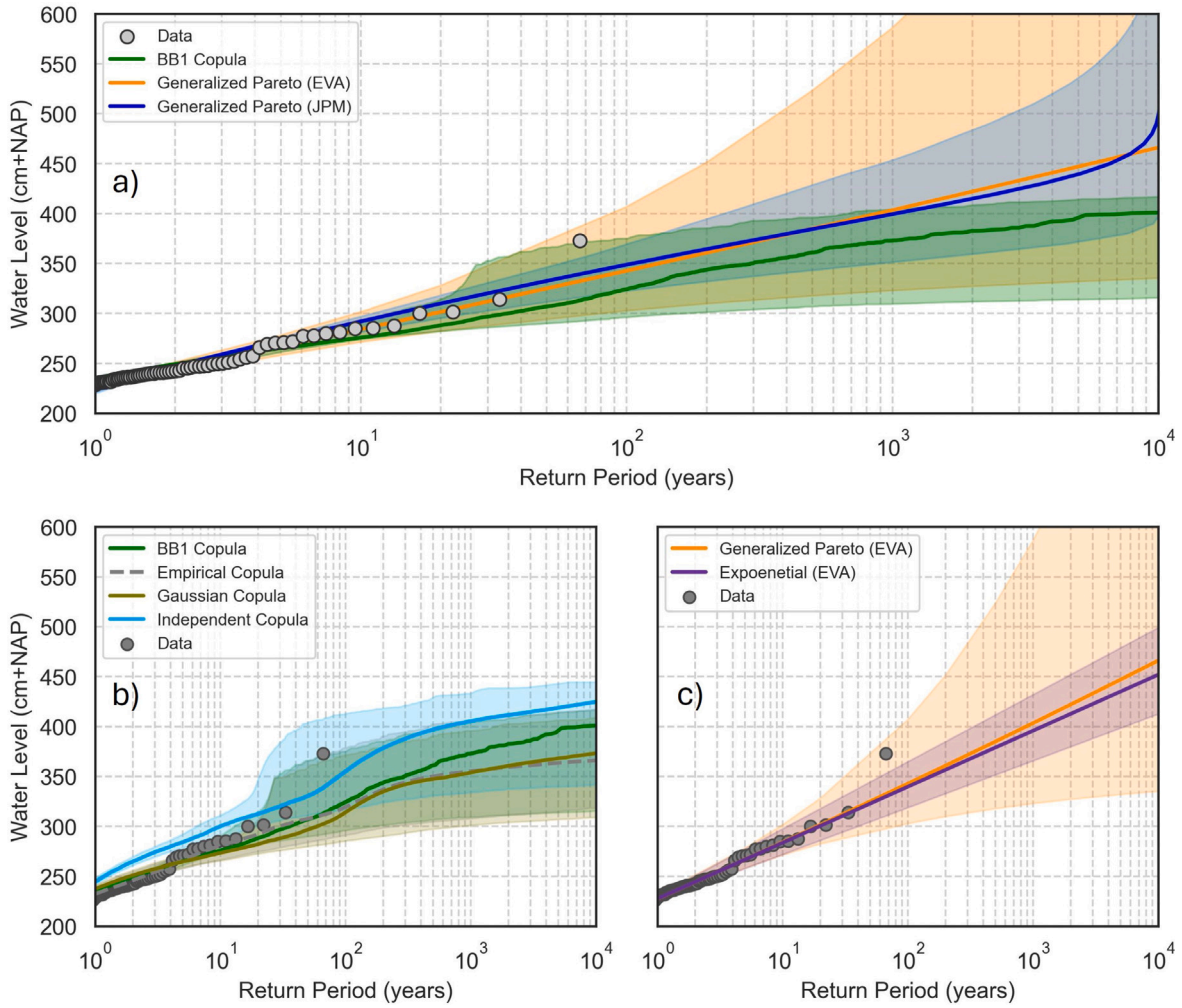

Fig. 14. Illustration of the results of different statistical methods for the estimation of EWL. The shaded areas show the 95% Confidence Interval. Panel (a) shows the comparison between the results from copulas, EVA and JPM, while panel (b) focuses on the differences of dependent and independent copulas. In panel (c), the Generalized Pareto (GP) and Exponential distributions are compared.

6. Conclusions

The revision of flood risk management plans and the maintenance of hydraulic structures call for better estimations of the projected EWLs. This study shows that a deeper investigation of their components could improve the understanding of EWLs providing robust inferences for them. EWLs analysed both from the perspective of water level dynamics as well as of water level extremes.

In the effort to reasonably estimate the declustering time for extreme storms, we used the main drivers of them e.g., SSP and wind speed. First, we identified the coherence between WL and SSP, finding an indicator of the assumption of declustering time equal to 4 days, based on the high coherence achieved for this period. After that, we calculated the time on which the highest correlation between extreme surges and peaks in wind speed data is achieved, to validate the selection of declustering time from the coherence analysis. Lastly we investigated the effect of the direction of the wind speed component on this correlation. Including the wind direction window the calculated correlation is higher which can explain the importance of this direction in the storm surges.

Additionally, by the spectral analysis, we tried to better describe the estuarine environment of Hoek van Holland station with the interaction of tides and specific conditions to lead in high amplitudes of sub-daily components. Moreover, the man-made interventions that affected the MSL are referenced as well as the influence of sea level rise until the end of our data is taken into consideration.

In the comparison between the dependence or independence of NTR and tides using copulas, it is shown that the latter one overestimates the EWL on both lower and higher quantiles. The selection of the right copula, based on their characteristics i.e. tail dependence and symmetry, to express this dependence highly affects the extrapolation. In our case the negative dependence is properly captured by the rotated (270 degrees) BB1 asymmetric copula, which outperforms traditional statistical methods for extremes, such as EVA and JPM. At the same time, the copula allows to account for the dependence between the assumed components of the EWLs. Consequently, the investigation of dependence between WL components using copulas, could improve the characterization of extreme WLs that lead to flood events in deltas.

CRediT authorship contribution statement

Faidon Diakomopoulos: Writing – original draft, Visualization, Methodology, Investigation, Conceptualization. **Alessandro Antonini:** Writing – review & editing, Visualization, Supervision, Methodology, Conceptualization. **Alexander Maria Rogier Bakker:** Writing – review & editing, Supervision, Methodology, Conceptualization. **Laura Maria Stancanelli:** Writing – review & editing, Supervision, Conceptualization. **Markus Hrachowitz:** Writing – review & editing, Supervision, Conceptualization. **Elisa Ragno:** Writing – review & editing, Supervision, Methodology, Investigation, Conceptualization.

Declaration of competing interest

The authors declare that they have no known competing financial interests or personal relationships that could have appeared to influence the work reported in this paper.

Data availability

Data will be made available on request.

Acknowledgements

This work is part of the Perspectief research programme Future flood risk management technologies for rivers and coasts with project number P21-23. This programme is financed by Domain Applied and Engineering Sciences of the Dutch Research Council (NWO) under grant No. C71A35. The authors would like to thank the editors and the anonymous reviewers for their valuable insights during the review process.

Appendix A. Supplementary data

Supplementary material related to this article can be found online at https://doi.org/10.1016/j.coastaleng.2024.104603.

References

Antonini, A., Raby, A., Brownjohn, J.M.W., Pappas, A., D'Ayala, D., 2019. Survivability assessment of fastnet lighthouse. Coast. Eng. 150, 18–38. http://dx.doi.org/10.1016/j.coastaleng.2019.03.007.

Arns, A., Wahl, T., Wolff, C., Vafeidis, A.T., Haigh, I.D., Woodworth, P., Niehüser, S., Jensen, J., 2020. Non-linear interaction modulates global extreme sea levels, coastal flood exposure, and impacts. Nat. Commun. 11 (1), 1918. http://dx.doi.org/10.1038/s41467-020-15752-5.

Caires, S., 2011. Extreme value analysis: Still water level. JCOMM Tech. Rep. (58), Geneva, Switzerland: World Meteorological Organization, Intergovernmental Oceanographic Commission (of UNESCO).

Coles, S., Bawa, J., Trenner, L., Dorazio, P., 2001. An introduction to statistical modeling of extreme values, vol. 208, Springer, http://dx.doi.org/10.1007/978-1-4471-3675-0.

Davison, A.C., Smith, R.L., 1990. Models for exceedances over high thresholds. J. R. Stat. Soc. Ser. B Stat. Methodol. 52 (3), 393–425, https://www.jstor.org/stable/2345667.

Day, Jr., J.W., Templet, P., 1989. Consequences of sea level rise: implications from the Mississippi Delta. Ocean & Coastal Management 17 (3), 241–257. http://dx.doi.org/10.1080/08920758909362088.

De Luca, G., Rivieccio, G., 2023. Modeling and simulating rainfall and temperature using rotated bivariate copulas. Hydrology 10 (12), 236. http://dx.doi.org/10.3390/hydrology10120236.

Diermanse, F., Roscoe, K., de la Cruz, J.L., Steenbergen, H., Vrouwenvelder, T., 2013. Hydra ring scientific documentation. Deltares Rep..

Dillingh, D., De Haan, L., Helmers, R., Können, G., Van Malde, J., 1993. De basispeilen langs de nederlandse kust: Statistisch onderzoek. DGW-93.023 rapport Dienst Getijdewateren.

Dookie, I., Rocke, S., Singh, A., Ramlal, C.J., 2018. Evaluating wind speed probability distribution models with a novel goodness of fit metric: a trinidad and tobago case study. Int. J. Energy Environ. Eng. 9, 323–339. http://dx.doi.org/10.1007/s40095-018-0271-y.

Ferrarin, C., Lionello, P., Orlić, M., Raicich, F., Salvadori, G., 2022. Venice as a paradigm of coastal flooding under multiple compound drivers. Sci. Rep. 12 (1), 5754. http://dx.doi.org/10.1038/s41598-022-09652-5.

Geerse, C., 2020. Interaction between tide and surge-modelling the tide evolution of the residual surge. HKV Consult. Final Rep..

Geerse, C., Rongen, G., Strijker, B., 2019. Schematization of storm surges-analysis based on simulated KNMI-data. HKV Consult. Final Rep..

Grases, A., Gracia, V., García-León, M., Lin-Ye, J., Sierra, J.P., 2020. Coastal flooding and erosion under a changing climate: implications at a low-lying coast (Ebro Delta). Water 12 (2), 346. http://dx.doi.org/10.3390/w12020346.

Gräwe, U., Burchard, H., Müller, M., Schuttelaars, H.M., 2014. Seasonal variability in M2 and M4 tidal constituents and its implications for the coastal residual sediment transport. Geophys. Res. Lett. 41 (15), 5563–5570. http://dx.doi.org/10.1002/2014GL060517.

Groeneweg, J., Caires, S., van Nieuwkoop, J., Bottema, M., 2022. A first assessment of the effect of storm climate trends and uncertainties on Dutch levee design. J. Flood Risk Manag. 15 (3), e12808. http://dx.doi.org/10.1111/jfr3.12808.

Guo, L., van der Wegen, M., Jay, D.A., Matte, P., Wang, Z.B., Roelvink, D., He, Q., 2015. River-tide dynamics: Exploration of nonstationary and nonlinear tidal behavior in the Yangtze River estuary. J. Geophys. Res.: Oceans 120 (5), 3499–3521.

Guo, L., Wang, Z.B., Townend, I., He, Q., 2019. Quantification of tidal asymmetry and its nonstationary variations. J. Geophys. Res.: Oceans 124 (1), 773–787. http://dx.doi.org/10.1029/2018JC014372.

Haigh, I.D., Marcos, M., Talke, S.A., Woodworth, P.L., Hunter, J.R., Hague, B.S., Arns, A., Bradshaw, E., Thompson, P., 2023. GESLA version 3: A major update to the global higher-frequency sea-level dataset. Geosci. Data J. 10 (3), 293–314. http://dx.doi.org/10.1002/gdj3.174.

Horsburgh, K., Wilson, C., 2007. Tide-surge interaction and its role in the distribution of surge residuals in the North Sea. J. Geophys. Res.: Oceans 112 (C8), http://dx.doi.org/10.1029/2006JC004033.

Hsiao, S.-C., Chiang, W.-S., Jang, J.-H., Wu, H.-L., Lu, W.-S., Chen, W.-B., Wu, Y.-T., 2021. Flood risk influenced by the compound effect of storm surge and rainfall under climate change for low-lying coastal areas. Sci. Total Environ. 764, 144439. http://dx.doi.org/10.1016/j.gloplacha.2005.07.004.

Katsman, C.A., Sterl, A., Beersma, J., Van den Brink, H., Church, J., Hazeleger, W., Kopp, R., Kroon, D., Kwadijk, J., Lammersen, R., et al., 2011. Exploring high-end scenarios for local sea level rise to develop flood protection strategies for a low-lying delta—the Netherlands as an example. Clim. Change 109, 617–645. http://dx.doi.org/10.1007/s10584-011-0037-5.

Kendall, M.G., 1938. A new measure of rank correlation. Biometrika 30 (1/2), 81–93. http://dx.doi.org/10.2307/2332226.

Kendall, M.G., 1975. Rank correlation methods. Griffin, London. Kendall MG.

KNMI, 2024. Hoe hoog zijn de stormvloeden die onze zeedijken moeten keren? URL https://www.knmi.nl/over-het-knmi/nieuws/hoe-hoog-zijn-de-stormvloeden-die-onze-zeedijken-moeten-keren.

Kollu, R., Rayapudi, S.R., Narasimham, S., Pakkurthi, K.M., 2012. Mixture probability distribution functions to model wind speed distributions. Int. J. Energy Environ. Eng. 3, 1–10. http://dx.doi.org/10.1186/2251-6832-3-27.

Krupskii, P., Joe, H., 2013. Factor copula models for multivariate data. J. Multivariate Anal. 120, 85–101. http://dx.doi.org/10.1016/j.jmva.2013.05.001.

Lee, E.-J., Kim, K., Park, J.-H., 2022. Reconstruction of long-term sea-level data gaps of tide gauge records using a neural network operator. Front. Marine Sci. 9, 1037697. http://dx.doi.org/10.3389/fmars.2022.1037697.

Liu, J.C., Lence, B.J., Isaacson, M., 2010. Direct joint probability method for estimating extreme sea levels. J. Waterway, Port, Coastal, Ocean Eng. 136 (1), 66–76. http://dx.doi.org/10.1061/(ASCE)0733-950X(2010)136:1(66).

Mann, H.B., 1945. Nonparametric tests against trend. Econometrica 245–259. http://dx.doi.org/10.2307/1907187.

Martín, A., Wahl, T., Enriquez, A.R., Jane, R., 2024. Storm surge time series declustering using correlation analysis. Weather Clim. Extrem. 100701. http://dx.doi.org/10.1016/j.wace.2024.100701.

Masina, M., D'Ayala, D., Antonini, A., 2022. Variations in monthly maximum gust speed at St Mary's, Isles of Scilly (UK). Earth Space Sci. 9 (11), http://dx.doi.org/10.1029/2022EA002380, e2022EA002380.

Medvedev, I., Kulikov, E., Rabinovich, A., 2017. Tidal oscillations in the Caspian Sea. Oceanology 57, 360–375. http://dx.doi.org/10.1134/S0001437017020138.

Medvedev, I.P., Vilibić, I., Rabinovich, A.B., 2020. Tidal resonance in the Adriatic Sea: Observational evidence. J. Geophys. Res.: Oceans 125 (8), http://dx.doi.org/10.1029/2020JC016168, e2020JC016168.

Munk, W., Zetler, B., Groves, G., 1965. Tidal cusps. Geophys. J. Int. 10 (2), 211–219. http://dx.doi.org/10.1111/j.1365-246X.1965.tb03062.x.

Naderi, A., Siadatmousavi, S.M., 2023. Extreme value analysis for waves in the Persian Gulf: Skill assessment of different methods for a fetch-limited basin. Reg. Stud. Mar. Sci. 59, 102812. http://dx.doi.org/10.1016/j.rsma.2023.102812.

Neumann, B., Vafeidis, A.T., Zimmermann, J., Nicholls, R.J., 2015. Future coastal population growth and exposure to sea-level rise and coastal flooding-a global assessment. PLoS One 10 (3), e0118571.

Nicholls, R.J., 1995. Coastal megacities and climate change. GeoJournal 37, 369–379. http://dx.doi.org/10.1007/BF00814018.

Nicholls, R.J., Wong, P.P., Burkett, V., Woodroffe, C.D., Hay, J., 2008. Climate change and coastal vulnerability assessment: scenarios for integrated assessment. Sustain. Sci. 3, 89–102. http://dx.doi.org/10.1007/s11625-008-0050-4.

Nienhuis, J.H., Van de Wal, R.S., 2021. Projections of global delta land loss from sea-level rise in the 21st century. Geophys. Res. Lett. 48 (14), http://dx.doi.org/10.1029/2021GL093368, e2021GL093368.

Northrop, P.J., Attalides, N., Jonathan, P., 2017. Cross-validatory extreme value threshold selection and uncertainty with application to ocean storm severity. J. R. Stat. Soc. Ser. C. Appl. Stat. 66 (1), 93–120. http://dx.doi.org/10.1111/rssc.12159.

Paalvast, P., 2014. Ecological studies in a man-made estuarine environment, the port of Rotterdam (Ph.D. thesis). http://dx.doi.org/10.13140/2.1.1101.6486, [Sl]:[Sn].

Pattiaratchi, C., 2011. Coastal tide gauge observations: dynamic processes present in the Fremantle record. pp. 185–202. http://dx.doi.org/10.1007/978-94-007-0332-27, Operational Oceanography in the 21st century.

Pawlowicz, R., Beardsley, B., Lentz, S., 2002. Classical tidal harmonic analysis including error estimates in MATLAB using T_TIDE. Comput. Geosci. 28 (8), 929–937.

Prestes, Y.O., Silva, A.C., Rollnic, M., Rosário, R.P., 2017. The M2 and M4 tides in the pará river estuary. Trop. Oceanogr. 45 (1), 1679–3013. http://dx.doi.org/10.5914/tropocean.v45i1.15198.

Proudman, J., 1955a. The effect of friction on a progressive wave of tide and surge in an estuary. Proc. R. Soc. A 233 (1194), 407–418, https://www.jstor.org/stable/99898.

Proudman, J., 1955b. The propagation of tide and surge in an estuary. Proc. R. Soc. A 231 (1184), 8–24. http://dx.doi.org/10.1098/rspa.1955.0153.

Pugh, D.T., Vassie, J., 1978. Extreme sea levels from tide and surge probability. In: Coastal Engineering 1978. pp. 911–930. http://dx.doi.org/10.9753/icce.v16.52.

Raby, A., Antonini, A., Pappas, A., Dassanayake, D., Brownjohn, J., D'Ayala, D., 2019. Wolf rock lighthouse: past developments and future survivability under wave loading. Phil. Trans. R. Soc. A 377 (2155), 20190027. http://dx.doi.org/10.1098/rsta.2019.0027.

Ragno, E., AghaKouchak, A., Cheng, L., Sadegh, M., 2019. A generalized framework for process-informed nonstationary extreme value analysis. Adv. Water Resour. 130, 270–282. http://dx.doi.org/10.1016/j.advwatres.2019.06.007.

Ragno, E., AghaKouchak, A., Love, C.A., Cheng, L., Vahedifard, F., Lima, C.H., 2018. Quantifying changes in future intensity-duration-frequency curves using multimodel ensemble simulations. Water Resour. Res. 54 (3), 1751–1764. http://dx.doi.org/10.1002/2017WR021975.

Ragno, E., Antonini, A., Pasquali, D., 2023. Investigating extreme sea level components and their interactions in the Adriatic and Tyrrhenian Seas. Weather Clim. Extrem. 41, 100590. http://dx.doi.org/10.1016/j.wace.2023.100590.

Reimann, L., Vafeidis, A.T., Honsel, L.E., 2023. Population development as a driver of coastal risk: Current trends and future pathways. Camb. Prisms: Coast. Futures 1, e14. http://dx.doi.org/10.1017/cft.2023.3.

Rossiter, J.R., 1961. Interaction between tide and surge in the Thames. Geophys. J. Int. 6 (1), 29–53. http://dx.doi.org/10.1111/j.1365-246X.1961.tb02960.x.

Sánchez-Arcilla, A., Jiménez, J.A., Valdemoro, H.I., Gracia, V., 2008. Implications of climatic change on spanish Mediterranean low-lying coasts: The Ebro delta case. J. Coast. Res. 24 (2), 306–316. http://dx.doi.org/10.2112/07A-0005.1.

Sartini, L., Antonini, A., 2024. On the spectral wave climate of the French Atlantic Ocean. Ocean Eng. 304, 117900. http://dx.doi.org/10.1016/j.oceaneng.2024.117900.

Sen, P.K., 1968. Estimates of the regression coefficient based on Kendall's tau. J. Amer. Statist. Assoc. 63 (324), 1379–1389. http://dx.doi.org/10.1080/01621459.1968.10480934.

Sklar, A., 1973. Random variables, joint distribution functions, and copulas. Kybernetika 9 (6), 449–460, http://dml.cz/dmlcz/125838.

Solari, S., Egüen, M., Polo, M.J., Losada, M.A., 2017. Peaks over threshold (POT): A methodology for automatic threshold estimation using goodness of fit p-value. Water Resour. Res. 53 (4), 2833–2849. http://dx.doi.org/10.1002/2016WR019426.

Spicer, P., Huguenard, K., Ross, L., Rickard, L.N., 2019. High-frequency tide-surge-river interaction in estuaries: Causes and implications for coastal flooding. J. Geophys. Res.: Oceans 124 (12), 9517–9530. http://dx.doi.org/10.1029/2019JC015466.

Stijnen, J., Kanning, W., Jonkman, S., Kok, M., 2014. The technical and financial sustainability of the Dutch polder approach. J. Flood Risk Manag. 7 (1), 3–15. http://dx.doi.org/10.1111/jfr3.12022.

Teixeira, R., Nogal, M., O'Connor, A., 2018. On the suitability of the generalized Pareto to model extreme waves. J. Hydraul. Res. 56 (6), 755–770. http://dx.doi.org/10.1080/00221686.2017.1402829.

Teng, F., Fang, G., Xu, X., Zhu, Y., 2023. Shallow water tides induced by frictional nonlinearity in the Bohai and Yellow Seas. J. Sea Res. 194, 102411. http://dx.doi.org/10.1016/j.seares.2023.102411.

Thomson, R.E., Emery, W.J., 2014. Data Analysis Methods in Physical Oceanography. Newnes.

Van Alphen, J., Haasnoot, M., Diermanse, F., 2022. Uncertain accelerated sea-level rise, potential consequences, and adaptive strategies in the Netherlands. Water 14 (10), 1527. http://dx.doi.org/10.3390/w14101527.

Van den Brink, H.W., de Goederen, S., 2017. Recurrence intervals for the closure of the Dutch Maeslant surge barrier. Ocean Sci. 13 (5), 691–701. http://dx.doi.org/10.5194/os-13-691-2017.

Van Ledden, M., Van den Berg, N., De Jong, M., Van Gelder, P., Heijer, C., Vrijling, J., Jonkman, S., Roos, P., Hulscher, S., Lansen, A., 2014. An idealized meteorological-hydrodynamic model for exploring extreme storm surge statistics in the North Sea. In: 34th International Conference on Coastal Engineering, ICCE 2014. Coastal Engineering Research Council, pp. 1–12. http://dx.doi.org/10.9753/icce.v34.management.21.

Wahl, T., Haigh, I.D., Nicholls, R.J., Arns, A., Dangendorf, S., Hinkel, J., Slangen, A.B., 2017. Understanding extreme sea levels for broad-scale coastal impact and adaptation analysis. Nat. Commun. 8 (1), 16075. http://dx.doi.org/10.1038/ncomms16075.

Weisse, R., von Storch, H., Niemeyer, H.D., Knaack, H., 2012. Changing north sea storm surge climate: An increasing hazard? Ocean & Coastal Management 68, 58–68. http://dx.doi.org/10.1016/j.ocecoaman.2011.09.005.

Williams, J., Horsburgh, K.J., Williams, J.A., Proctor, R.N., 2016. Tide and skew surge independence: New insights for flood risk. Geophys. Res. Lett. 43 (12), 6410–6417. http://dx.doi.org/10.1002/2016GL069522.

Woodruff, J.D., Irish, J.L., Camargo, S.J., 2013. Coastal flooding by tropical cyclones and sea-level rise. Nature 504 (7478), 44–52. http://dx.doi.org/10.1038/nature12855.

Woodworth, P.L., Melet, A., Marcos, M., Ray, R.D., Wöppelmann, G., Sasaki, Y.N., Cirano, M., Hibbert, A., Huthnance, J.M., Monserrat, S., et al., 2019. Forcing factors affecting sea level changes at the coast. Surv. Geophys. 40 (6), 1351–1397. http://dx.doi.org/10.1007/s10712-019-09531-1.

Yue, S., Wang, C.Y., 2002. Applicability of prewhitening to eliminate the influence of serial correlation on the Mann-Kendall test. Water Resour. Res. 38 (6), 1–4. http://dx.doi.org/10.1029/2001WR000861.

Yue, S., Wang, C., 2004. The Mann-Kendall test modified by effective sample size to detect trend in serially correlated hydrological series. Water Resour. Manag. 18 (3), 201–218. http://dx.doi.org/10.1023/B:WARM.0000043140.61082.60.